

Model-Free Measurement of Local Entropy Production and Extractable Work in Active Matter

Sunghan Ro^{1,*}, Buming Guo^{2,*}, Aaron Shih³, Trung V. Phan⁴, Robert H. Austin⁵, Dov Levine^{1,†}, Paul M. Chaikin^{2,‡}, and Stefano Martiniani^{1,2,3,4,6,§}

¹Department of Physics, Technion-Israel Institute of Technology, Haifa 3200003, Israel

²Center for Soft Matter Research, Department of Physics, New York University, New York 10003, USA

³Courant Institute of Mathematical Sciences, New York University, New York 10003, USA

⁴Department of Chemical Engineering and Materials Science, University of Minnesota, Minneapolis, Minnesota 55455, USA

⁵Department of Physics, Princeton University, Princeton 08544, New Jersey, USA

⁶Simons Center for Computational Physical Chemistry, Department of Chemistry, New York University, New York 10003, USA



(Received 22 April 2022; accepted 9 September 2022; published 21 November 2022)

Time-reversal symmetry breaking and entropy production are universal features of nonequilibrium phenomena. Despite its importance in the physics of active and living systems, the entropy production of systems with many degrees of freedom has remained of little practical significance because the high dimensionality of their state space makes it difficult to measure. Here we introduce a local measure of entropy production and a numerical protocol to estimate it. We establish a connection between the entropy production and extractability of work in a given region of the system and show how this quantity depends crucially on the degrees of freedom being tracked. We validate our approach in theory, simulation, and experiments by considering systems of active Brownian particles undergoing motility-induced phase separation, as well as active Brownian particles and *E.coli* in a rectifying device in which the time-reversal asymmetry of the particle dynamics couples to spatial asymmetry to reveal its effects on a macroscopic scale.

DOI: 10.1103/PhysRevLett.129.220601

Time reversal symmetry breaking (TRSB) in active matter systems arises from the self-propelled motion of individual particles, driven by the continuous injection of energy into the system [1–4]. TRSB is linked to the emergence of steady-state currents in phase space, a clear signature of a system's departure from equilibrium, which can be quantified in terms of the global rate of entropy production [5–13].

Notwithstanding its importance, global entropy production has not yet found a place in the routine characterization of experimental many-body nonequilibrium systems. The reasons for this are twofold. First, the high-dimensional nature of phase space has hindered the estimation of entropy production beyond low-dimensional systems [14–18]. Although multiple approaches have been adopted to mitigate this problem from a variety of perspectives [19–22], an adequate solution remains elusive.

The second, and arguably more fundamental, reason is that global entropy production is a single number which, as such, cannot provide insight into the complex patterns of TRSB events occurring in many-body systems. Crucial theoretical insight into this problem came from Nardini *et al.* [23] who, moving beyond the estimation of the global quantity, proposed a spatially local decomposition of entropy production. To this end, they analyzed stochastic field theories of active model systems undergoing motility-induced phase separation (MIPS) showing that at a coarse-grained level

TRSB events are pronounced at the interfaces while reversibility is partially recovered in bulk, thus casting light on where the system's departure from equilibrium is more prominent. However, the dynamics of local degrees of freedom obtained by coarse-graining are in many cases non-Markovian [17,24], which makes the accurate estimation of the local entropy production difficult.

To overcome this problem, we introduce a universal information-theoretic measure and a numerical protocol to estimate it. Our approach does not require knowledge of the equations of motion, enabling the analysis of experimental systems. Furthermore, our method does not require information about the memory time of the process, allowing the evaluation of local entropy production even in systems following non-Markovian dynamics. We then apply this protocol to several theoretical and experimental systems. We show that the measured local entropy production provides comprehensive information about the nature of TRSB events in the system, such as their characteristic length scales, as well as whether any work can be extracted when an external mechanism is weakly coupled to the tracked degrees of freedom.

Local entropy production rate.—To make these ideas concrete, we start by introducing the concept of local entropy production in an example of active Brownian particles (ABPs) with excluded volume interactions. The ABPs propel

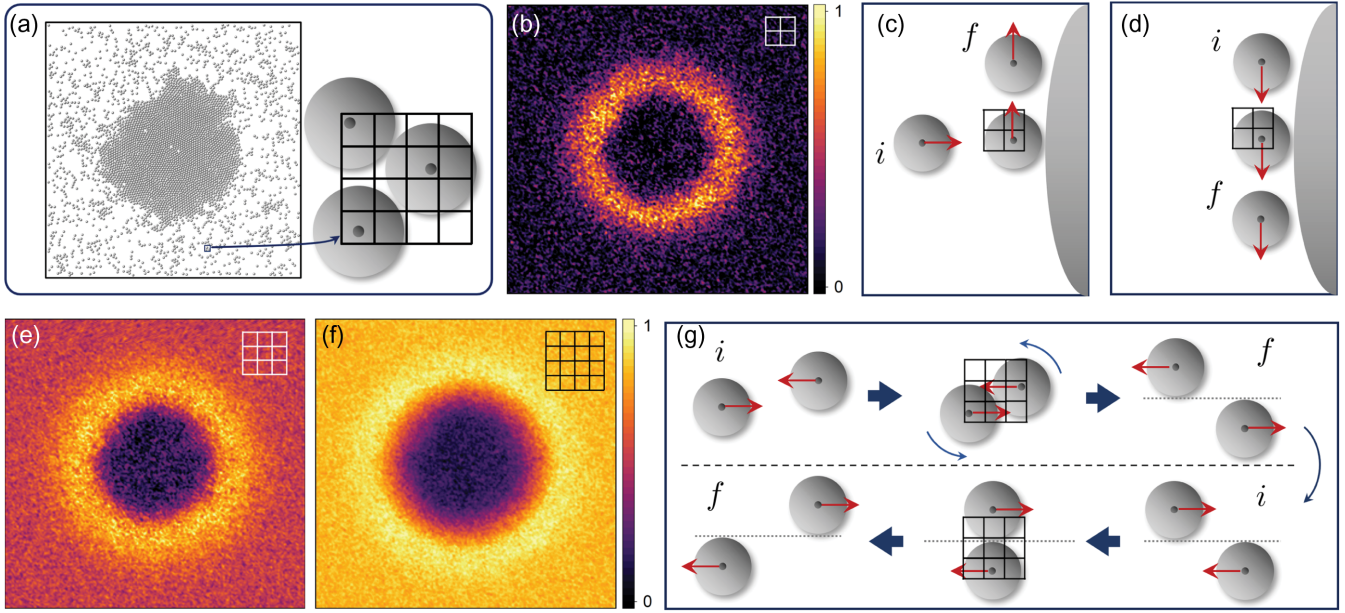


FIG. 1. Normalized local entropy production rate, EP, for a MIPS cluster. (a) ABP presenting MIPS in simulation. (b) EP with 2×2 blocks. (c) Typical motion of an ABP approaching an interface. (d) Typical motion of an ABP propelling parallel to the interface. (e) and (f) EP with 3×3 and 4×4 blocks, that capture progressively more degrees of freedom and EP in the dilute phase. (g) TRSB of two ABPs colliding with each other. Normalization factors for EPs are chosen so that the fraction of samples with EPs greater than these factors is less than 10^{-3} . Specifically, we set the factors as (b) 2.3×10^{-3} , (e) 7.8×10^{-3} , and (f) 2.7×10^{-2} .

themselves at a constant speed, with a direction that diffuses randomly. Remarkably, for high enough speed, ABPs accumulate and form a dense cluster even when the particles do not attract each other; this is MIPS [see Fig. 1(a) for a snapshot].

Since ABPs are not in equilibrium, entropy is constantly produced by the system. To measure entropy production (EP), we track the system configuration $X(t)$, consisting of both positions and orientations, over a given observation interval τ , yielding the global state trajectory X . Because of a lack of time reversal symmetry in the system dynamics, we expect the time-reversed trajectory X^R obtained by playing X backward to be distinguishable from the original forward trajectory. Accordingly, the global EP can be quantified by the Kullback-Leibler (KL) divergence between the forward and the backward realizations of the trajectories: $\sigma = \tau^{-1} \langle \ln(\mathcal{P}[X]/\mathcal{P}[X^R]) \rangle$, where $\mathcal{P}[X]$ is the probability density function (PDF) of X in the forward dynamics, and the angled brackets denote the average over $\mathcal{P}[X]$.

The global EP is a single positive number whose nonzero value only signifies that the system is out of equilibrium. This obscures the spatial inhomogeneity of the system; for example, we expect distinctive patterns of nonequilibrium particle motion in the dense phase, in the dilute phase, and at the interface between them, which the global EP is insensitive to. To recover this information, we turn to measuring the local EP by overlaying an $L \times L$ square grid over the system and specifying local states by observing the particle occupancy in a small block chosen from the grid.

We set the grid size so that only one particle can fit in a 2×2 block to ensure fine enough spatial resolution, precluding multiple occupancy and ambiguity in the particle motion [25]. We then associate each grid point with the state of a 2×2 block, for which there are five possible configurations: either empty or one of the four sites is being occupied. We denote this local state at time t as $\chi_i(t)$ where the index $i = (x, y)$ specifies the position of the block. Tracking $\chi_i(t)$ yields a local trajectory χ_i , with which we define the local EP

$$\sigma_i = \frac{1}{\tau} \langle \ln(\mathcal{P}[\chi_i]/\mathcal{P}[\chi_i^R]) \rangle, \quad (1)$$

where χ_i^R is the time-reversed realization of the local trajectory and $\mathcal{P}[\chi_i]$ is the PDF of the local trajectory.

Using the measure of EP that we will introduce presently, we evaluated σ_i for a range of positions i , yielding a spatially resolved map showing local EP. In Fig. 1(b), we show this map for local states defined by the occupancy of 2×2 blocks, showing that the local EP is pronounced at the interface between the condensed and dilute phases. To understand this, consider the typical motion of a particle from an initial state i to a final state f near an interface, as depicted in Fig. 1(c). If a particle approaches the interface from a normal direction, it is likely to stay at the contact location while propelling toward the droplet center. When the propulsion direction reorients itself so that it becomes roughly parallel to the interface, the particle will move away from the contact location. The time-reversed

realization of this event is highly unlikely, as a particle moving along the interface is likely to pass by without any abrupt turns, as depicted in Fig. 1(d). This imbalance leads to high local EP measured at the interface. Note that this result is in agreement with the field-theoretic predictions [23,34,35], which we reproduce for active model *B* in the Supplemental Material [26].

Importantly, due to the size of the grid, information from 2×2 blocks can only detect TRSB events that depend on the dynamics of a single particle, and is insensitive to events that depend explicitly on the dynamics of multiple particles. To study these, we next compute local EP in larger regions, using blocks which can track two or more particles simultaneously [see Fig. 1(a)]. The local EP obtained with 3×3 blocks shown in Fig. 1(e) still presents the highest EP at the interface, but there is also considerable entropy production in the dilute phase. EP in the dilute phase originates from irreversible collision events between two particles, as shown in the upper portion of Fig. 1(g). Because of the persistence of the propulsion, colliding ABPs slide along each other until their propulsion directions become perpendicular to the line connecting their centers, at which point the particles go past each other. If we reverse the propulsion directions of the particles from the final state, we will not observe the time-reversed realization of the forward trajectory as depicted in the lower portion of Fig. 1(g). Further enlarging the block size to 4×4 reveals even more EP in the dilute phase and a marginal increase of EP in the dense phase, as seen in Fig. 1(f). These examples demonstrate that local EPs measured with various choices of local states may enable characterization of nonequilibrium events occurring in a variety of systems.

In the Supplemental Material [26], we provide local EP measurement results based on particle positions and orientations. In this case, we observe that tracking 1×1 blocks is sufficient to capture TRSB events at the interface, while tracking 2×2 blocks is sufficient to highlight the distinction between the dense and the dilute phases. We further show that EP of ABPs measured with our method agrees with the analytical result given in Ref. [8] and also report that similar results are reproduced with active particles strictly on lattice.

Measure of entropy production rate.—We now proceed to the problem of how to actually measure local EP as defined in Eq. (1). As is evident from the equation, direct evaluation would require the PDF of the local state trajectories $\mathcal{P}[\chi_i]$. Obtaining $\mathcal{P}[\chi_i]$ is, however, a daunting task since the local dynamics exhibit a finite memory due to interactions between the local degrees of freedom and their environment [36].

To address this problem, we propose a measure based on the information-theoretic quantity known as *cross-parsing complexity*, \mathcal{C} , introduced by Ziv and Merhav [36,37]. The aim of cross parsing is to compress a *sample* sequence using substrings taken from a *database* sequence. More intuitively,

consider a sample sequence $\mathbf{Y} = (012101110230)$ and a database $\mathbf{Z} = (301201110310)$. We sequentially draw the longest consecutive array of symbols from the sample that can also be found in the database, leading to the parsing $(012, 10, 1110, 2, 30)$. The resulting number of substrings is the cross-parsing complexity, which is $\mathcal{C}(\mathbf{Y} \parallel \mathbf{Z}) = 5$ in our example.

Next, consider the case when \mathbf{Y} and \mathbf{Z} are sequences of length N randomly drawn from two different ensembles with probabilities $P_Y(\mathbf{Y})$ and $P_Z(\mathbf{Z})$, respectively. In this case, the cross-parsing complexity has been shown to satisfy [36]

$$\lim_{N \rightarrow \infty} \left(\frac{\ln N}{N} \mathcal{C}(\mathbf{Y} \parallel \mathbf{Z}) + \frac{1}{N} \sum_X P_Y(X) \ln P_Z(X) \right) = 0.$$

Therefore, the cross-entropy rate S_{YZ} of P_Y from P_Z is

$$S_{YZ} = \lim_{N \rightarrow \infty} \frac{\ln N}{N} \mathcal{C}(\mathbf{Y} \parallel \mathbf{Z}). \quad (2)$$

A more general version of this result is derived from coding theory in the Supplemental Material [26]. Intuitively, \mathcal{C} is small if the sample and the database sequences are similar, thus yielding a small cross-entropy rate, while dissimilar sequences lead to large \mathcal{C} and thus a large cross-entropy rate. When $P_Z = P_Y$ we simply recover the entropy rate S_Y .

Recall that the local entropy production is the KL divergence between the forward sequence χ_i and the backward sequence χ_i^R . Since the KL divergence of P_Y from P_Z is $S_{YZ} - S_Y$, using Eq. (2) we find that the difference of the cross-parsing complexity between independently sampled forward and backward sequences, $\mathcal{C}(\chi_i' \parallel \chi_i^R)$, and between independently sampled forward sequences, $\mathcal{C}(\chi_i' \parallel \chi_i)$, gives the entropy produced in an observation interval,

$$\tilde{\sigma}_i = \lim_{N \rightarrow \infty} \frac{\ln N}{N} [\mathcal{C}(\chi_i' \parallel \chi_i^R) - \mathcal{C}(\chi_i' \parallel \chi_i)], \quad (3)$$

which is the measure (estimator) that we propose. An estimator of this kind was originally proposed by Ziv and Merhav [36] using cross parsing and Lempel-Ziv factorization (viz., lossless data compression) to estimate the cross entropy and entropy, respectively. Roldán and Parrondo [20,38] tested the Ziv-Merhav estimator on physical systems alongside refinements of the approach. They reported large error and slow convergence of the estimators which make them impractical. We recognize that the large error stems from mixing cross parsing and compression and suggest a symmetric construction solely using cross parsing. In the Supplemental Material [26], we show that our measure exhibits significantly faster convergence than previous approaches, thus enabling the analysis presented in Fig. 1.

In terms of numerical complexity, \mathcal{C} can be obtained efficiently in $\mathcal{O}(N)$ time using suffix arrays [39]. Importantly, Eq. (3) can be computed without prior

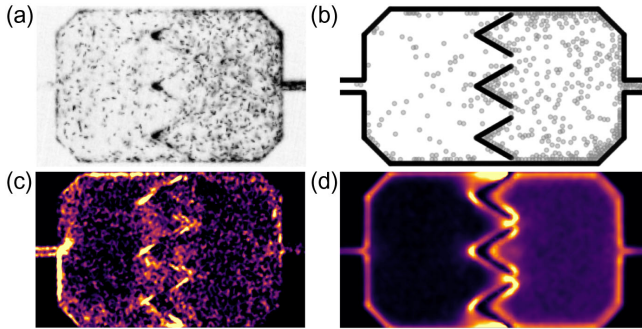


FIG. 2. Local entropy production of *E. coli* [snapshot in (a) and EP in (c)] and ABPs [snapshot in (b) and EP in (d)] in a rectifying cell. In the lower panels, the EP is captured with 2×2 blocks, with a brighter color indicating larger EP. The particle distributions show higher particle density on the right side of the cell driven by the funnels and particle accumulations along the walls.

knowledge about memory time. Finally, we note that Eq. (3) is defined for a discrete sequence, so we must subsample a continuous time trajectory by a time interval τ yielding a discrete sequence of length N . We thus estimate the local EP of Eq. (1) by computing $\sigma_i = \tilde{\sigma}_i/\tau$, which would be valid for small enough τ .

Application to experiments.—Our procedure is applicable to physical and biological systems as well as to simulations. In Fig. 2, we show a snapshot of an experimental system in which *E. coli* are circulating in chambers where funnels rectify the bacterial motion, creating flows and density heterogeneity. We also show an analogous simulation with ABPs. Using the same protocol as in Fig. 1, with 2×2 blocks, we see in the lower panels that the entropy production is largest at the funnel tips where the particle trajectories bifurcate, and at the boundaries [40].

Work extraction.—It remains to connect local entropy production with other physical quantities. We start by noting that the local EP is *not* proportional to the heat dissipated by the local degrees of freedom [2,41,42]. We next employ a simple model to argue that our measured local EP is directly related to the work that can be extracted from a given region of the system.

To this end, we consider a work extraction mechanism and show that our measure captures which degrees of freedom must be coupled to in order to extract net work. Extracting work from active matter has received much attention recently [43–46], and our protocol is particularly relevant in this context. Specifically, we consider a run-and-tumble particle (RTP) on a ring with four discrete sites with lattice spacing a [Fig. 3(a)], coupled to a thermal reservoir with constant temperature T . The particle flips randomly between two orientations and jumps to the neighboring sites either driven by thermal noise or by a thrust \mathbf{f} exerted along its orientation. We impose the local detailed balance condition to the particle motion, and the thrust makes forward motion more likely than backward motion, thus leading to TRSB [26]. For this model, we measure the EP for three different degrees of freedom: (i) the state of the entire system X , (ii) the particle occupancy χ_n on two adjacent sites, and (iii) the particle occupancy and orientation χ_s on the same sites.

The results for the three measurements are shown in Fig. 3(b). As expected, we observe dramatic dependence of the EP on the choice of degrees of freedom. The global EP, estimated by tracking X (blue triangles), fully recovers the entropy production measured by accounting for the heat dissipation (solid blue line). In contrast, the local EP for χ_s (black squares) only partially captures the global EP, while the local EP obtained by tracking χ_n (red circles) is zero, since the resulting trajectory is time symmetric.

We now argue that the local EP is directly related to the amount of work that can be extracted by coupling to the tracked degree of freedom. That is, if a mechanism is weakly coupled to the degree of freedom with a small coupling strength γ , work can be extracted at the linear order in γ only if a positive EP is obtained when tracking the degrees of freedom in the unperturbed state. To illustrate this, we consider an RTP with an asymmetric “key” fixed to its head. As shown in Figs. 3(d)–3(f), we introduce two turnstile-like mechanisms, one that couples to χ_n , the other to χ_s . Both mechanisms extract work when rotating counterclockwise, while releasing energy when

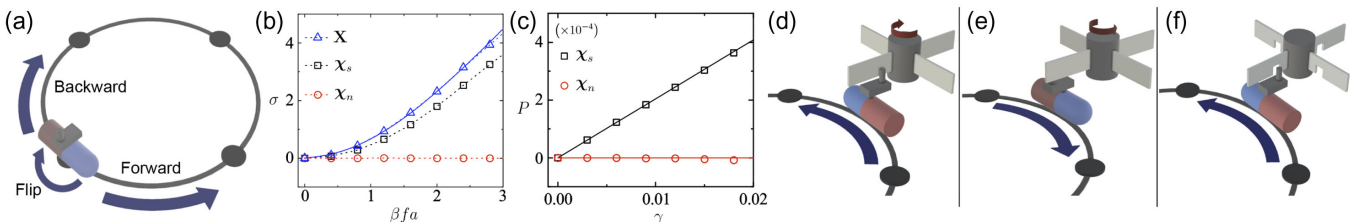


FIG. 3. Entropy production and work extraction. (a) Schematic figure of the toy model and its motions. (b) EP measured with full information X (blue triangles), occupancy and particle orientation on two sites χ_s (black squares), and occupancy on two sites χ_n (red circles). The total entropy increases by $f a/T$ for forward motion, and decreases by the same amount for backward motion, with f the propulsion force, a the lattice constant, and T the temperature of the bath. (c) The power $P \equiv \langle W \rangle / \tau$ extracted by the work extraction mechanisms shown in (d)–(f) when $\ln(w_f/w_b) = \beta f a = 0.25$, where w_f and w_b are the forward and backward rates and $\beta = (k_B T)^{-1}$. Solid lines are exact results [26]. Shown in (d) and (e) is the mechanism coupling to χ_n , while the mechanism shown in (f) couples to χ_s .

rotating clockwise. The mechanism shown in Figs. 3(d) and 3(e) couples to χ_n and rotates whenever the particle moves between two sites where the turnstile arm is placed. In contrast, the mechanism depicted in Fig. 3(f) is orientation specific—the turnstile rotates with the particle when it is oriented in a clockwise direction, but does not interact with the particle otherwise, as depicted in Fig. 3(f); it thus couples to χ_s . The power harnessed is shown in Fig. 3(c), plotted with respect to γ , and clearly shows that the mechanism coupled to χ_n (red circles) does not harness work, while for the mechanism coupled to χ_s (black squares) the work extracted is linearly increasing with γ and thus finite.

This observation can be generalized to any degrees of freedom coupled weakly to a work extraction mechanism based on nonequilibrium linear response theory [47]. Given that the system is weakly perturbed by the mechanism, the average power recorded by the mechanism during a time interval t is given by $\langle P \rangle = (\gamma/2)\langle \sigma(\chi) \tilde{W}(\chi) \rangle_\chi + \mathcal{O}(\gamma^2)$, where $\sigma(\chi)$ and $\gamma \tilde{W}(\chi)$ are EP and the work extracted by the mechanism, respectively, for a particular realization of χ [26,41]. Note that $\tilde{W}(\chi)$ is of order $\mathcal{O}(\gamma^0)$ for small γ , and the angled brackets indicate averaging over the steady-state measure for χ . Since entropy production is strictly zero for any time-symmetric trajectory, this equation indicates that the average extractable work is zero if the (local) EP measured for χ is zero. [48].

To conclude, we have introduced a protocol to measure local EP by devising an effective information-theoretic measure, and demonstrated it on several numerical and experimental systems. We have shown that it is possible to identify which regions of the system are driven out of equilibrium in simulations and experiments, how these depend on the degrees of freedom being tracked, and their relation to the locally extractable work. These results show that the local EP is a universal and powerful tool for studying nonequilibrium many-body systems, which extends recent efforts to apply tools of information theory to study physical systems [51–53]. Note that our approach can be applied even if the governing equations of the systems are not known, and that it can reveal nonequilibrium features in experimental systems even when the signature of TRSB is hidden in fluctuations. It would be interesting to apply our method to study various aspects of glassy dynamics, biological systems, and externally driven systems.

We thank Yariv Kafri for useful and insightful discussions, and Elsen Tjhung for clarifications regarding the field theoretic simulations. We thank Maria Jose Reyes for preparation of the figures. This work was supported by the National Science Foundation (NSF) Physics of Living Systems (Award No. 1504867). S. M. acknowledges support from the Simons Foundation Faculty Fellowship and from the Simons Center for Computational Physical

Chemistry at NYU, as well as partial support from the National Science Foundation (Award No. 2226387 and 2039575). D. L. thanks the U.S.-Israel Binational Science Foundation (Grant No. 2014713) and the Israel Science Foundation (Grant No. 1866/16). P. M. C. acknowledges support from the Simons Society of Fellows, as well as partial support from the Materials Research Science and Engineering Center (MRSEC) Program of the NSF under Award No. 1420073 for data analysis. P. M. C. and B. G. were partially supported by DOE SC-0020976 for numerical simulations. S. R. and D. L. were also supported by the National Research Foundation of Korea (2019R1A6A3A03033761). R. H. A. and T. V. P. were supported by the NSF through the Center for the Physics of Biological Function (Award No. 1734030). This work was supported in part through the NYU IT High Performance Computing, and the Minnesota Supercomputing Institute, resources, services, and staff expertise.

^{*}These authors contributed equally to this work.

[†]dovlevine19@gmail.com

[‡]chaikin@nyu.edu

[§]sm7683@nyu.edu

- [1] M. C. Marchetti, J.-F. Joanny, S. Ramaswamy, T. B. Liverpool, J. Prost, M. Rao, and R. A. Simha, *Rev. Mod. Phys.* **85**, 1143 (2013).
- [2] É. Fodor, R. L. Jack, and M. E. Cates, *Annu. Rev. Condens. Matter Phys.* **13**, 215 (2022).
- [3] J. O’Byrne, Y. Kafri, J. Tailleur, and F. van Wijland, *Nat. Rev. Phys.* **4**, 167 (2022).
- [4] J. Tailleur and M. E. Cates, *Phys. Rev. Lett.* **100**, 218103 (2008).
- [5] U. Seifert, *Rep. Prog. Phys.* **75**, 126001 (2012).
- [6] C. Van den Broeck and M. Esposito, *Physica (Amsterdam)* **418**, 6 (2015).
- [7] D. Mandal, K. Klymko, and M. R. DeWeese, *Phys. Rev. Lett.* **119**, 258001 (2017).
- [8] S. Shankar and M. C. Marchetti, *Phys. Rev. E* **98**, 020604 (R) (2018).
- [9] F. S. Gnesotto, F. Mura, J. Gladrow, and C. P. Broedersz, *Rep. Prog. Phys.* **81**, 066601 (2018).
- [10] J. Kurchan, *J. Phys. A* **31**, 3719 (1998).
- [11] J. L. Lebowitz and H. Spohn, *J. Stat. Phys.* **95**, 333 (1999).
- [12] U. Seifert and T. Speck, *Europhys. Lett.* **89**, 10007 (2010).
- [13] C. Jarzynski, *Annu. Rev. Condens. Matter Phys.* **2**, 329 (2011).
- [14] D. Andrieux, P. Gaspard, S. Ciliberto, N. Garnier, S. Joubaud, and A. Petrosyan, *Phys. Rev. Lett.* **98**, 150601 (2007).
- [15] J. Li, J. M. Horowitz, T. R. Gingrich, and N. Fakhri, *Nat. Commun.* **10**, 1666 (2019).
- [16] G. Manzano, D. Subero, O. Maillet, R. Fazio, J. P. Pekola, and É. Roldán, *Phys. Rev. Lett.* **126**, 080603 (2021).
- [17] D. J. Skinner and J. Dunkel, *Proc. Natl. Acad. Sci. U.S.A.* **118** (2021).

- [18] P. Pietzonka and U. Seifert, *J. Phys. A: Math. Theor.* **51**, 01LT01 (2018).
- [19] J. Liphardt, S. Dumont, S. B. Smith, I. Tinoco, and C. Bustamante, *Science* **296**, 1832 (2002).
- [20] E. Roldán and J. M. R. Parrondo, *Phys. Rev. E* **85**, 031129 (2012).
- [21] C. Battle, C. P. Broedersz, N. Fakhri, V. F. Geyer, J. Howard, C. F. Schmidt, and F. C. MacKintosh, *Science* **352**, 604 (2016).
- [22] D.-K. Kim, Y. Bae, S. Lee, and H. Jeong, *Phys. Rev. Lett.* **125**, 140604 (2020).
- [23] C. Nardini, É. Fodor, E. Tjhung, F. van Wijland, J. Tailleur, and M. E. Cates, *Phys. Rev. X* **7**, 021007 (2017).
- [24] I. A. Martínez, G. Bisker, J. M. Horowitz, and J. M. Parrondo, *Nat. Commun.* **10**, 3542 (2019).
- [25] We have verified that the grid spacing we choose is fine enough to capture the pattern of EP by confirming that the pattern is unaltered by choosing a finer discretization. See the Supplemental Material [26] for details.
- [26] See Supplemental Material at <http://link.aps.org/supplemental/10.1103/PhysRevLett.129.220601> for additional analytical derivations, numerical results, computational and experimental details, which also includes Refs. [27–33].
- [27] Y. Fily and M. C. Marchetti, *Phys. Rev. Lett.* **108**, 235702 (2012).
- [28] J. A. Anderson, J. Glaser, and S. C. Glotzer, *Comput. Mater. Sci.* **173**, 109363 (2020).
- [29] M. R. Banerjee, S. Succi, S. Ansumali, and R. Adhikari, *J. Stat. Mech.* (2017) 103202.
- [30] U. Seifert, *Phys. Rev. Lett.* **95**, 040602 (2005).
- [31] Z. Zhou, T. Zhou, S. Zhang, Z. Shi, Y. Chen, W. J. Wan, X. X. Li, X. Z. Chen, S. N. G. Corder, Z. L. Fu, L. Chen, Y. Mao, J. C. Cao, F. G. Omenetto, M. K. Liu, H. Li, and T. H. Tao, *Adv. Sci.* **5**, 1700982 (2018).
- [32] F. Viela, M. Mathelié-Guinlet, A. Viljoen, and Y. F. Dufrêne, *Mol. Microbiol.* **113**, 683 (2020).
- [33] S. K. DeWitt and E. A. Adelberg, *Genetics* **47**, 577 (1962).
- [34] R. Wittkowski, A. Tiribocchi, J. Stenhammar, R. J. Allen, D. Marenduzzo, and M. E. Cates, *Nat. Commun.* **5**, 4351 (2014).
- [35] D. Martin, J. O’Byrne, M. E. Cates, É. Fodor, C. Nardini, J. Tailleur, and F. van Wijland, *Phys. Rev. E* **103**, 032607 (2021).
- [36] J. Ziv and N. Merhav, *IEEE Trans. Inf. Theory* **39**, 1270 (1993).
- [37] A. D. Wyner, J. Ziv, and A. J. Wyner, *IEEE Trans. Inf. Theory* **44**, 2045 (1998).
- [38] E. Roldán and J. M. R. Parrondo, *Phys. Rev. Lett.* **105**, 150607 (2010).
- [39] J. Kärkkäinen, D. Kempa, and S. J. Puglisi, in *Annual Symposium on Combinatorial Pattern Matching* (Springer, New York, 2013), pp. 189–200.
- [40] In the ABP simulation, larger EP is also observed in the higher density region on the right of the funnels due to TRSB collision events. Such a pattern is less pronounced in the bacterial experiment as the chamber is three-dimensional and therefore irreversible collisions are less frequent.
- [41] G. E. Crooks and S. Still, *Europhys. Lett.* **125**, 40005 (2019).
- [42] É. Fodor and M. E. Cates, *Europhys. Lett.* **134**, 10003 (2021).
- [43] P. Pietzonka, É. Fodor, C. Lohrmann, M. E. Cates, and U. Seifert, *Phys. Rev. X* **9**, 041032 (2019).
- [44] T. Ekeh, M. E. Cates, and É. Fodor, *Phys. Rev. E* **102**, 010101(R) (2020).
- [45] T. Speck, *Europhys. Lett.* **114**, 30006 (2016).
- [46] T. Speck, *Europhys. Lett.* **123**, 20007 (2018).
- [47] C. Maes, *Front. Phys.* **8**, 229 (2020).
- [48] If χ were Markovian, alternatively, one could have arrived at the same conclusion from the thermodynamic uncertainty relation, $\langle \tilde{W}(\chi) \rangle^2 \leq \text{Var}[\tilde{W}(\chi)]S(\chi)$ [49,50].
- [49] A. C. Barato and U. Seifert, *Phys. Rev. Lett.* **114**, 158101 (2015).
- [50] J. M. Horowitz and T. R. Gingrich, *Phys. Rev. E* **96**, 020103(R) (2017).
- [51] S. Martiniani, P. M. Chaikin, and D. Levine, *Phys. Rev. X* **9**, 011031 (2019).
- [52] R. Avinery, M. Kornreich, and R. Beck, *Phys. Rev. Lett.* **123**, 178102 (2019).
- [53] S. Martiniani, Y. Lemberg, P. M. Chaikin, and D. Levine, *Phys. Rev. Lett.* **125**, 170601 (2020).